A reduced-order-model Bayesian obstacle detection algorithm

Mahadevan Ganesh and Stuart C. Hawkins

Abstract We develop an efficient Bayesian algorithm for solving the inverse problem of classifying and locating certain two dimensional objects using noisy far field data obtained by illuminating them with a radiating wave. While application of Bayesian algorithms for wave-propagation inverse problems is itself innovative, the principal novelty in this work is in using i) a surrogate Bayesian posterior distribution computed using a generalised polynomial chaos approximation; and ii) an efficient wave-propagation-specific reduced order model in place of the full multiple scattering forward model. We demonstrate the capability of this approach with simulations in which we accurately detect two dimensional objects, with shapes motivated by safety and security applications.

1 Introduction

The time harmonic radiating field u scattered by a two dimensional scatterer D in a homogeneous medium satisfies the Helmholtz partial differential equation (PDE)

$$\triangle u + k^2 u = 0, \qquad \underline{x} \in \mathbb{R}^2 \setminus \overline{D}, \tag{1}$$

and the Sommerfeld radiation condition [5, Equation (3.85)]

$$\lim_{r\to\infty} \sqrt{r}\left(\frac{\partial u}{\partial r} - iku\right) = 0, \qquad r = |\underline{x}|, \tag{2}$$

M. Ganesh
Colorado School of Mines, Golden, CO 80401, USA, e-mail: mganesh@mines.edu

Stuart C. Hawkins
Macquarie University, Sydney, NSW 2109, Australia, e-mail: stuart.hawkins@mq.edu.au

uniformly for all directions θ. Here $k = 2\pi/\lambda$ is the wavenumber and λ is the wavelength. The two dimensional Helmholtz model—which arises in scattering of acoustic or electromagnetic waves by cylinders, whereupon D represents the cross section of the cylinder—is often used as a proving ground for developing scattering algorithms. The approach used in this paper generalises to the three dimensional case and application to the three dimensional case will be the subject of a future work.

The radiating scattered field is induced by an incident field via a boundary condition imposed on the boundary ∂D of the scatterer D. Our approach allows all of the standard wave propagation boundary conditions. For the numerical experiments considered in Section 3, we impose the Dirichlet boundary condition

$$u(\underline{x}) = -u^{\mathrm{i}}(\underline{x}), \qquad \underline{x} \in \partial D, \tag{3}$$

which models acoustic scattering by a sound soft body, or electromagnetic scattering by a perfect electrical conductor under transverse electric (TE) incident polarisation. In this work we assume the incident field is generated by a point source located at a point $\underline{x}_0$ close to the body D. The incident field is then

$$u^{\mathrm{i}}(\underline{x}) = \frac{i}{4} H_0^{(1)}(|\underline{x} - \underline{x}_0|), \tag{4}$$

where $H_n^{(1)}$ denotes the first kind Hankel function of order n.

A consequence of the Sommerfeld radiation condition (2) is that at large distances from the body the scatterered field satisfies

$$u(r,\theta) \approx \frac{e^{ikr}}{\sqrt{r}} u^{\infty}(\theta). \tag{5}$$

The modulation function u^{∞} is known as the far field pattern of D. The well known radar cross section, which is important in applications, is computed from $|u^{\infty}|$ and is a measure of the strength of the reflection from D. The complex valued far field additionally includes phase information, which is important in our algorithm.

In practice the far field u^{∞} is dependent on the shape of the body D. In many applications the shape of D (or a close approximation to it) can be described by a finite

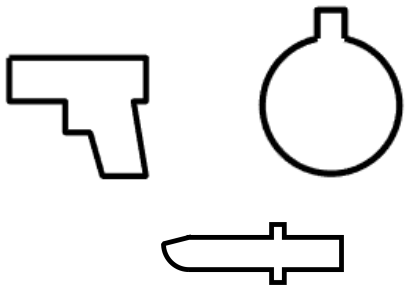

Fig. 1 Visualisations of the reference scatterers: a gun (left), a bomb (right) and a knife (bottom).

number of parameters. An important example is the case where D is a configuration of disjoint objects, which can be parametrised by choosing a local origin with coordinates (x,y) inside each object, and describing the one dimensional boundary of the object in local polar coordinates (r,θ). For star-shaped objects the shape is determined by the function $r(\theta)$ and this function can itself be discretised using standard functional analysis techniques such as Fourier series or spline approximation so that the scatterer is described by a vector parameter.

Such an approach has been used in various applications in science and engineering to describe or reconstruct the shape of a single object [10, 17, 20, 5, 21]. However, if the aim is to detect objects that match certain known shapes in a catalogue (such as in Figure 1) then the object shape can be parametrised using an integer (an index into the catalogue) and the configuration of J obstacles is described using $d = 3J$ parameters. Such inverse problems are of interest in security detection type applications. Motivated by such applications, we assume that D is described by the vector parameter $\underline{\sigma} \in \mathbb{R}^d$, and we denote the corresponding far field $u^\infty(\theta;\underline{\sigma})$.

It is convenient to define $F(\underline{\sigma}) = u^\infty(\cdot;\underline{\sigma})$. The problem of computing $F(\underline{\sigma})$ for a given $\underline{\sigma}$ is commonly known as the *forward problem*. Given data $\underline{\widehat{y}}$ the corresponding *inverse problem* is to find $\underline{\sigma}$ such that

$$F(\underline{\sigma}) = \widehat{y}. \tag{6}$$

Typically the data $\widehat{y}$ incorporates noise and so may not be in the range of F. This is one of the classical wave propagation inverse problems and has received considerable attention in the literature (see the book [5] and references therein). The substantial literature for the ill-posed wave-propagation inverse problem is based on a deterministic approach using Tikhonov regularisation techniques.

A completely different approach is to formulate the deterministic inverse problem (6) as a stochastic problem in which the parameter $\underline{\sigma}$ is modelled as a stochastic variable with associated probability distribution $\rho_0(\underline{\sigma}) = \rho_0^1(\sigma_1)\rho_0^2(\sigma_2)\cdots\rho_0^d(\sigma_d)$. The d-dimensional distribution is known in the Bayesian setting as the prior. Under the assumption that the noise in the data is random with probability distribution ρ, the noisy data can be written in the form

$$\widehat{y} = y + \eta. \tag{7}$$

Here y is in the range of F and η is a d-dimensional sample of the random noise. Then Bayes' Theorem gives an improved probability distribution for $\underline{\sigma}$ conditional on the data $\widehat{y}$,

$$\rho_{\widehat{y}}(\underline{\sigma}) = \frac{\rho(\widehat{y} - F(\underline{\sigma}))\,\rho_0(\underline{\sigma})}{Z} \tag{8}$$

where

$$Z = \int_\Omega \rho(\widehat{y} - F(\underline{\sigma}))\,\rho_0(\underline{\sigma})\,d\underline{\sigma}, \tag{9}$$

and $\Omega = \Omega_1 \times \cdots \times \Omega_d \subseteq \mathbb{R}^d$ is the domain of the stochastic variable $\underline{\sigma}$. The distribution $\rho_{\widehat{y}}$ is known in the Bayesian setting as the posterior. This approach was

introduced, in the context of PDEs, with justification using mathematical theory, in the seminal paper [24]. The use of Bayesian inversion for PDEs has been mostly limited to simple diffusion problems [24, 28, 14, 16] posed on a bounded domain, for which the associated forward problem can be solved efficiently using the finite element method, with fast evaluation using techniques such as the multigrid method. For this simple class of PDEs, fast evaluation justifies the use of Bayesian techniques. The application of Bayesian inversion to wave propagation has been limited to two dimensional acoustic models for shape reconstruction [25, 2, 20, 21, 6].

In practice we discretise by requiring that (6) holds at discrete points $\theta_1,\dots,\theta_M \in [0,2\pi)$, leading to

$$\underline{F}(\underline{\sigma}) = \underline{\widehat{y}}, \tag{10}$$

where

$$\underline{F}(\underline{\sigma}) = (F^{(m)}(\underline{\sigma}))_{m=1,\dots,M}, \qquad F^{(m)}(\underline{\sigma}) = u^{\infty}(\theta_m;\underline{\sigma}), \tag{11}$$
$$\underline{\widehat{y}} = (\widehat{y}_m)_{m=1,\dots,M}, \qquad \widehat{y}_m = \widehat{y}(\theta_m).$$

Solving (10) to determine D is extremely challenging, even when D is known to be a simply connected body in a known location, because the number of parameters d required to parametrise the body is large, and the corresponding posterior probability distribution (8) is d-dimensional.

In view of the above, it is not feasible to use this approach to determine the shapes of several obstacles—that is, when D comprises several disjoint bodies—located in a large area. However, if specific information is available about the shapes of the obstacles then the number of parameters required to parametrise D may be substantially reduced. In this work we consider the case where D comprises two bodies D_1 and D_2 which are chosen from a catalogue of three known shapes, and whose centres lie in bounded rectangular regions S_1 and S_2 respectively. The shapes in the catalogue are visualised in Figure 1. Under these assumptions $D(\underline{\sigma}) = D_1(\underline{\sigma}) \cup D_2(\underline{\sigma})$ can be parametrised by

$$\underline{\sigma} = (\sigma_1,\dots,\sigma_6) = (x_1,y_1,x_2,y_2,s_1,s_2) \tag{12}$$

where $(x_j,y_j) \in S_j \subseteq \mathbb{R}^2$ are the coordinates of the center of D_j and $s_j \in \{1,2,3\}$ identifies the shape of D_j. Such problems arise in several applications in which the aim is to determine whether or not certain objects are present in a particular area. This model can be extended to include changes of scale, in which the scatterers' diameters are changed but their shapes remain the same, by adding the scaling factor as an extra parameter.

2 Efficient approximation of the forward model

The posterior distribution (8) contains rich information about the body D. However, even for the simplified model, this information is hard to access because the poste-

rior distribution is defined on a $d = 6$ dimensional stochastic space. In practice, information about the posterior is typically extracted by sampling using Markov Chain Monte Carlo (MCMC) methods, computing conditional- and marginal-posterior distributions, or by computing the modal value. All of these approaches require a large number of evaluations of the posterior using (8), which in turn requires a large number of evaluations of the forward model (11).

Because the forward problem involves computing the far field, it is desirable to use surface integral based methods such as boundary element methods (BEM), which satisfy the radiation condition (2) exactly and for which the far field is readily available. However, for obstacles comprising heterogeneous materials or irregular shapes, such as the shapes in the catalogue (see Figure 1), application of BEM is challenging. In this work we couple a high order finite element method (FEM) with a high order Nyström BEM. The high-order coupled FEM-BEM scheme [1, 13] facilitates handling general materials and shapes using the FEM whilst properly incorporating the radiation condition (2) using the BEM.

2.1 gPC approximation

Evaluating the forward model (11) using the coupled FEM-BEM is typically time consuming, requiring a few seconds CPU time on a modern workstation even for simple cases, so that evaluating the posterior (8) at thousands of points is prohibitively expensive. To facilitate fast evaluation of the posterior (8) at thousands of points we replace the forward model in (8) with its generalised polynomial chaos (gPC) approximation. A similar approach has been used for diffusion problems [18, 22, 3, 4] and the resulting posterior—computed using the gPC approximation in place of the full forward model—is sometimes known as a surrogate posterior. Our degree L gPC approximation is

$$\underline{F}_L(\underline{\sigma}) = (F_L^{(m)}(\underline{\sigma}))_{m=1,\dots,M}, \qquad F_L^{(m)}(\underline{\sigma}) = \sum_{|\underline{l}|\le L} c_{\underline{l}}^{(m)} Q_{\underline{l}}(\underline{\sigma}), \tag{13}$$

where $\underline{l} = (l_1,\dots,l_d)$ and $|\underline{l}| = \max_{j=1,\dots,d} l_j$. Here the tensor product polynomial chaos polynomials are

$$Q_{\underline{l}}(\underline{\sigma}) = Q_{l_1}^1(\sigma_1)\cdots Q_{l_d}^d(\sigma_d), \tag{14}$$

and for each $j = 1,\dots,d$ the polynomials $Q_0^j,\dots,Q_L^j$ are orthonormal with respect to the inner product on Ω_j induced by the prior distribution,

$$\langle f, g\rangle_j = \int_{\Omega_j} f(\sigma)\overline{g(\sigma)}\rho_0^j(\sigma)\,d\sigma. \tag{15}$$

The expansion coefficients are computed using

$$c_{\underline{l}}^{(m)} = \int_{\Omega} F^{(m)}(\underline{\sigma}) Q_{\underline{l}}(\underline{\sigma})\, d\underline{\sigma}. \tag{16}$$

In practice the integral in (16) is approximated with high order accuracy using an $(L+1)^d$ point tensor product Gauss quadrature rule.

Once the coefficients $c_{\underline{l}}^{(m)}$ have been computed for $m = 1,\ldots,M$ and $|\underline{l}| \leq L$ the gPC approximation (13) can be evaluated for a given $\underline{\sigma} \in \Omega$ very quickly. Thus a significant advantage of this approach is that the gPC approximation can be setup offline by computing and storing the coefficients (16) and subsequently evaluated online very quickly.

The gPC approximation is spectrally accurate, with convergence rate $\mathscr{O}(L^{-r})$, where r is the regularity constant of the forward model $\underline{F}$ with respect to the parameter $\underline{\sigma}$. It is well known [5] that the far field is smooth with respect to the spatial variable even for configurations with non-smooth obstacles. Because of its connection to the far field, as demonstrated in [9], the forward model $\underline{F}$ is smooth with respect to $\underline{\sigma}$. Thus in practice, for the model considered in this article, $L \leq 10$ is sufficient.

Next we describe an efficient reduced order model for the forward model with high-order accuracy. For the wave propagation problem, our approach facilitates efficient offline setup of the reduced order model, independent of $\sigma \in \mathbb{R}^d$.

2.2 Reduced order model

To compute the gPC coefficients using an $(L+1)^d$ point tensor product Gauss quadrature rule requires $(L+1)^d$ evaluations of the forward model (11). We accelerate setting up the gPC approximation by replacing the forward model in (16) with a reduced order model (ROM) approximation.

For the scattering problem in this work there is a well established ROM based on the T-matrix. For a single scatterer D with centre at the origin, the T-matrix ROM involves expanding the incident field in regular cylindrial wavefunctions,

$$u^{\mathrm{i}}(r,\theta) = \sum_{n=-\infty}^{\infty} a_n J_{|n|}(kr) e^{in\theta}. \tag{17}$$

Here J_n is the Bessel function of order n and the coefficients a_n for the incident wave are given explicitly by

$$a_n = H_{|n|}^{(1)}(kR) e^{in(\pi+\phi)}, \tag{18}$$

where (R,ϕ) are polar coordinates for the source location $\underline{x}_0$. The scattered field is expanded in radiating cylindrical wavefunctions

$$u(r,\theta) = \sum_{n=-\infty}^{\infty} b_n H_{|n|}^{(1)}(kr) e^{in\theta} \tag{19}$$

and from the linearity of the Helholtz equation (1) it follows that there is a matrix T such that

$$\mathrm{b} = \mathrm{T}\,\mathrm{a} \tag{20}$$

where $\mathrm{b} = (b_n)$, $\mathrm{a} = (a_n)$. The matrix T is called the T-matrix of D and encapsulates the scattering properties of D for *any* incident wave. In practice the series (17) and (19) are truncated for $|n| \leq N$ and the corresponding finite T-matrix has dimension $(2N+1) \times (2N+1)$. The truncation parameter N is chosen using Equation (12) in [11] and depends on the wavenumber k and the radius of D.

The T-matrix was introduced by Waterman in the 1960s [26, 27] and has been extensively used since (see [19] and references therein). The T-matrix is usually computed using the Null Field method, which is well known to be numerically unstable for scatterers that are large or have a large aspect ratio [23, 15]. In this work we use the numerically stable formulation [7],

$$T_{mn} = \frac{1}{4}\sqrt{\frac{k}{\pi}} i^{|m|}(1+i)\int_0^{2\pi} u_n^{\infty}(\theta) e^{-im\theta}\, d\theta \tag{21}$$

to compute the (single-scattering) T-matrix of each scatterer in the catalogue, where u_n^{∞} is the far field of the scatterer computed with incident field

$$u^{\mathrm{i}}(r,\theta) = J_{|n|}(kr)e^{in\theta}. \tag{22}$$

Once the T-matrix of each scatterer in the catalogue is available it can be efficiently used for an online multiple scattering computation to obtain the far field of $D(\underline{\sigma})$ using the approach in [8]. The error analysis in [12] establishes that the error in the far field computed using the T-matrix ROM is of the same order as the error obtained using the high-order coupled FEM-BEM solver. However, we emphasise that the T-matrices are independent of $\underline{\sigma}$ and so can be computed offline and stored before being used to computed the gPC coefficients in (16).

3 Numerical Results

We demonstrate our approach for configurations modelled stochastically by $D(\underline{\sigma}) = D_1(\underline{\sigma}) \cup D_2(\underline{\sigma})$ and parametrised as in (12) with

$$\begin{aligned} &x_1 = \sigma_1 \sim \mathscr{U}(-4,-2), \quad && y_1 = \sigma_2 \sim \mathscr{U}(-1,1), \quad && s_1 = \sigma_5 \sim \mathscr{U}\{1,2,3\}, \\ &x_2 = \sigma_3 \sim \mathscr{U}(2,4), && y_2 = \sigma_4 \sim \mathscr{U}(-1,1), && s_2 = \sigma_6 \sim \mathscr{U}\{1,2,3\}. \end{aligned}$$

The configuration is illuminated from above by a point source at $\underline{x}_0 = (0,7)$ with field given by (4). We choose the incident wavenumber $k = \pi$ so that the corresponding incident wavelength $\lambda = 2$ is about double the diameter of our test objects. (After scaling the dimensionless units we use in our numerical experiments, this corresponds to a wavelength a bit longer than used by Wi-Fi.)

In our numerical experiments we create test configurations $D(\underline{\sigma}_0)$ for samples $\underline{\sigma}_0$ of $\underline{\sigma}$. For each test configuration we generate far field data $\underline{y}$ with

$$y_m = u^\infty(\theta_m, \underline{\sigma}_0), \qquad m = 1, \ldots, M, \tag{23}$$

for $M = 20$ using the T-matrix based reduced order model described in Section 2. A detailed investigation to determine how many data points M are required to obtain an accurate reconstruction of the configuration will be the subject of a future work and is beyond the scope of this paper. We generate synthetic noisy data from $\underline{y}$ using (7) with 10% noise using

$$\eta_m \sim \mathcal{N}(0, \tau^2), \qquad \tau = 0.1|u^\infty(\cdot; \underline{\sigma}_0)|. \tag{24}$$

We avoid the "inverse crime" in which the data is generated using the same forward model that is used for the inversion (see [5, Page 154]) by generating our synthetic data using the T-matrix based reduced order model rather than using the gPC approximation, and by including random noise. The far field associated with a particular sample $\underline{\sigma}_0$ and the corresponding noisy data are visualised in Figure 2. The posterior $\rho_{\underline{\hat{y}}}(\cdot)$ has a six-dimensional domain comprising four dimensions associated with continuous random variables and two dimensions associated with discrete random variables. The posterior is computed using (8) with the forward model approximated using the gPC polynomial (13) for the four dimensions associated with continuous random variables. (gPC approximation is not required for the dimensions associated with the discrete random variables.) Because the random variables in our stochastic parametrisation are uniform, our gPC basis (14) uses dilated and translated Legendre polynomials. The gPC truncation parameter L was chosen so that the error in the gPC approximation (in the maximum norm) was at least of order 10^{-2}. In practice the maximum norm was approximated using 64 points.

Althought the posterior $\rho_{\underline{\hat{y}}}(\cdot)$ contains rich information about the configuration $D(\underline{\sigma}_0)$, in practice it is hard to extract this information due the high dimension of the domain Ω. In this work we observed that typically the sets $\Omega_\tau = \{\underline{\sigma} \in \Omega \ : \ \rho_{\underline{\hat{y}}}(\underline{\sigma}) \geq \tau\}$ for $\tau > 0$ have very small diameter. This indicates that the data allows us to accurately locate the centre of each scatterer. However the small diameter of these sets presents problems for Markov Chain Monte Carlo (MCMC) sampling because there is low probability that one of the samples lands in Ω_τ. We have found it useful to compute the marginal posterior density of σ_j,

$$\rho^{(j)}_{\underline{\hat{y}}}(\sigma_j) = \int_{\Omega_{-j}} \rho_{\underline{\hat{y}}}(\underline{\sigma})\, d\underline{\sigma}_{-j} \tag{25}$$

where

$$\underline{\sigma}_{-j} = (\sigma_1, \ldots, \sigma_{j-1}, \sigma_{j+1}, \ldots, \sigma_6), \qquad \Omega_{-j} = \Omega_1 \times \cdots \times \Omega_{j-1} \times \Omega_{j+1} \cdots \times \Omega_6.$$

In practice we approximate the integral in (25) using a tensor product Gauss-Legendre rule with $4L+1$ points in each dimension. In Figure 2 (left) we demon-

strate the accuracy of our method for detecting the location of the scatterers by visualising the marginal posterior densities of x_1, y_1, x_2, y_2 (respectively $\sigma_1, \ldots, \sigma_4$) computed using the data visualised in Figure 2 (right). Our visualisation includes a schematic of the configuration $D(\underline{\sigma}_0)$ and the corresponding total field. The corresponding marginal posterior probabilities for the shapes are visualised in Figure 3.

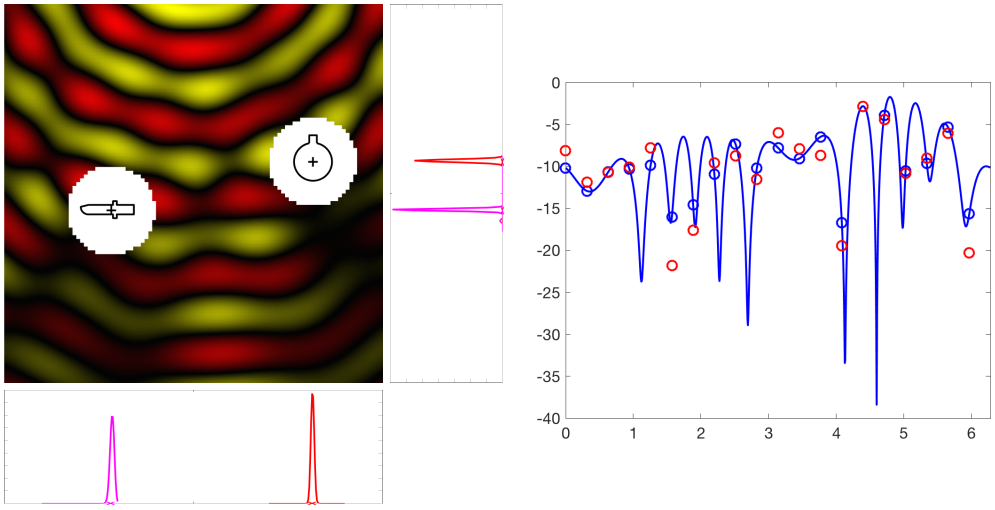

Fig. 2 Left: visualisation of the total field $u^{\mathrm{i}}(\cdot) + u(\cdot;\underline{\sigma})$ (main panel) and the marginal posteriors for the x and y coordinates of the left scatterer (magenta) and the right scatterer (red). Right: visualisation of the noisy data (red) and the originating cross section $10\log_{10} 2\pi|u^{\infty}(\cdot;\underline{\sigma})|^2$ (blue).

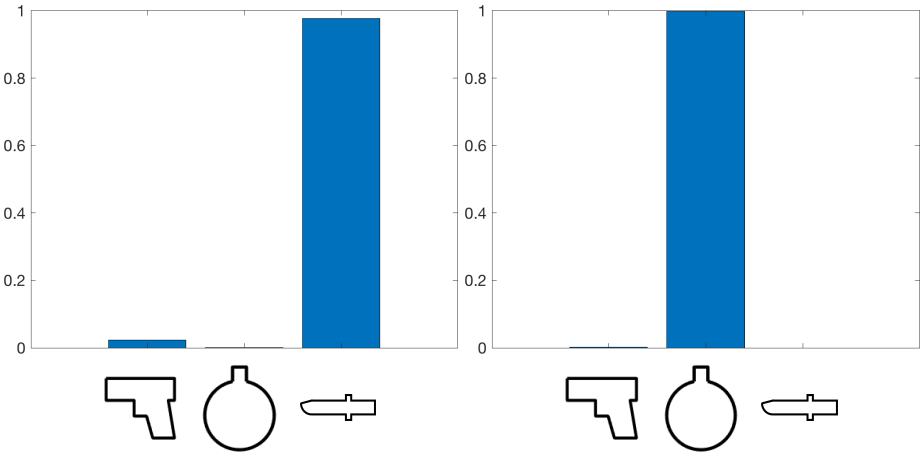

Fig. 3 Visualisation of the marginal posteriors for the shape of the left and right scatterers.

Acknowledgements SCH thanks Alistair Reid of Data61 for helpful discussions that guided part of this work.

References

1. Bagheri, S., Hawkins, S.C.: A coupled FEM-BEM algorithm for the inverse acoustic medium problem. ANZIAM **56**, C163–C178 (2015)
2. Bui-Thanh, T., Ghattas, O.: An analysis of infinite dimensional Bayesian inverse shape acoustic scattering and its numerical approximation. J. Uncertainty Quant. **2**, 203–222 (2014)
3. Chen, P., Schwab, C.: Sparse-grid, reduced-basis Bayesian inversion. Comput. Methods Appl. Mech. Engrg. **297**, 84–115 (2015)
4. Chen, P., Schwab, C.: Sparse-grid, reduced-basis Bayesian inversion: nonaffine-parametric nonlinear equations. J. Comput Phys. **316**, 470–503 (2016)
5. Colton, D., Kress, R.: Inverse Acoustic and Electromagnetic Scattering Theory, 3rd edn. Springer (2012)
6. Daza, M.L., Capistrán, M.A., Christen, J.A., Guadarrama, L.: Solution of the inverse scattering problem from inhomogeneous media using affine invariant sampling. Math. Meth. Appl. Sci. **40**, 3311–3319 (2017)
7. Ganesh, M., Hawkins, S.C.: A far-field based T-matrix method for two dimensional obstacle scattering. ANZIAM J. **51**, C201–C216 (2009)
8. Ganesh, M., Hawkins, S.C.: A stochastic pseudospectral and T-matrix algorithm for acoustic scattering by a class of multiple particle configurations. J. Quant. Spectrosc. Radiat. Transfer **123**, 41–52 (2013)
9. Ganesh, M., Hawkins, S.C.: A high performance computing and sensitivity analysis algorithm for stochastic many-particle wave scattering. SIAM J. Sci. Comput. **37**, A1475–A1503 (2015)
10. Ganesh, M., Hawkins, S.C.: Scattering by stochastic boundaries: hybrid low- and high-order quantification algorithms. ANZIAM J. **56**, C312–C338 (2016)
11. Ganesh, M., Hawkins, S.C.: Algorithm 975: TMATROM—a T-matrix reduced order model software. ACM Trans. Math. Softw. **44**, 9:1–9:18 (2017)
12. Ganesh, M., Hawkins, S.C., Hiptmair, R.: Convergence analysis with parameter estimates for a reduced basis acoustic scattering T-matrix method. IMA J. Numer. Anal. **32**, 1348–1374 (2012)
13. Ganesh, M., Morgenstern, C.: High-order FEM-BEM computer models for wave propagation in unbounded and heterogeneous media: Application to time-harmonic acoustic horn problem. J. Comp. Appl. Math. **37**, 183–203 (2016)
14. Jiang, L., Ou, N.: Multiscale model reduction for Bayesian inverse problems of subsurface flow. J. Comput. Appl. Math. **319**, 188–209 (2017)
15. Khlebtsov, N.: Anisotropic properties of plasmonic nanoparticles: depolarized light scattering, dichroism, and birefringence. J Nanophotonics **4**, 041,587–041,587 (2010)
16. Knapik, B.T., van der Vaart, A.W., van Zanten, J.H.: Bayesian recovery of the initial condition for the heat equation. Commun. Stat. **42**, 1294–1313 (2013)
17. Lamberg, L., Muinonen, K., Ylönen, J., Lumme, K.: Spectral estimation of Gaussian random circles and spheres. J. Comput. Appl. Math. **136**, 109–121 (2001). DOI 10.1016/S0377-0427(00)00578-1
18. Lu, F., Morzfeld, M., Chorin, A.J.: Limitations of polynomial chaos expansion in the Bayesian solution of inverse problems. J. Comput Phys. **282**, 138–147 (2015)
19. Mishchenko, M.I., et al.: Comprehensive thematic T-matrix reference database: A 2013–2014 update. J Quant Spectrosc Radiat Transfer **146**, 249–354 (2014)
20. Palafox, A., Capistrán, M.A., Christen, J.A.: Effective parameter dimension via Bayesian model selection in the inverse acoustic scattering problem. Math. Probl. Eng. **2014**, 1–12 (2014)

21. Palafox, A., Capistrán, M.A., Christen, J.A.: Point cloud-based scatterer approximation and affine invariant sampling in the inverse scattering problem. Math. Meth. Appl. Sci. **40**, 3393–3403 (2017)
22. Schillings, C., Schwab, C.: Sparse, adaptive Smolyak quadratures for Bayesian inverse problems. Inverse Problems **29**, 1–28 (2013)
23. Somerville, W.R.C., Auguié, B., Ru, E.C.L.: Severe loss of precision in calculations of T-matrix integrals. J Quant Spectrosc Radiat Transfer **113**, 524–535 (2012)
24. Stuart, A.: Inverse problems: A Bayesian perspective. Acta Numer. **19**, 451–559 (2010)
25. Wang, Y., Ma, F., Zheng, E.: Bayesian method for shape reconstruction in the inverse interior scattering problem. Math. Probl. Eng. **2015**, 1–12 (2015)
26. Waterman, P.C.: Matrix formulation of electromagnetic scattering. Proc. IEEE **53**, 805–812 (1965)
27. Waterman, P.C.: New formulation of acoustic scattering. J. Acoust. Soc. Am. **45**, 1417–1429 (1969)
28. Yang, K., Guha, N., Efendiev, Y., Mallick, B.: Bayesian and variational Bayesian approaches for flows in heterogeneous random media. J. Comput. Phys. **345**, 275–293 (2017)